



Review

A Review on Fusion Welding of Dissimilar Ferritic/Austenitic Steels: Processing and Weld Zone Metallurgy

Fabio Giudice ¹, Severino Missori ², Cristina Scolaro ³ and Andrea Sili ^{3,*}

¹ Department of Civil Engineering and Architecture, University of Catania, 95123 Catania, Italy; fabio.giudice@unict.it

² Department of Industrial Engineering, University of Rome-Tor Vergata, 00133 Roma, Italy; missori@uniroma2.it

³ Department of Engineering, University of Messina, 98166 Messina, Italy; cscolaro@unime.it

* Correspondence: asili@unime.it

Abstract: Dissimilar welds between ferritic and austenitic steels represent a good solution for exploiting the best performance of stainless steels at high and low temperatures and in aggressive environments, while minimizing costs. Therefore, they are widely used in nuclear and petrochemical plants; however, due to the different properties of the steels involved, the welding process can be challenging. Fusion welding can be specifically applied to connect low-carbon or low-alloy steels with high-alloy steels, which have similar melting points. The welding of thick plates can be performed with an electric arc in multiple passes or in a single pass by means of laser beam equipment. Since the microstructure and, consequently, the mechanical properties of the weld are closely related to the composition, the choice of the filler metal and processing parameters, which in turn affect the dilution rate, plays a fundamental role. Numerous technical solutions have been proposed for welding dissimilar steels and much research has developed on welding metallurgy; therefore, this article is aimed at a review of the most recent scientific literature on issues relating to the fusion welding of ferritic/austenitic steels. Two specific sections are dedicated, respectively, to electric arc and laser beam welding; finally, metallurgical issues, related to dilution and thermal field are debated in the discussion section.



Citation: Giudice, F.; Missori, S.; Scolaro, C.; Sili, A. A Review on Fusion Welding of Dissimilar Ferritic/Austenitic Steels: Processing and Weld Zone Metallurgy. *J. Manuf. Mater. Process.* **2024**, *8*, 96. <https://doi.org/10.3390/jmmp8030096>

Academic Editor: Hui Huang

Received: 19 March 2024

Revised: 16 April 2024

Accepted: 1 May 2024

Published: 4 May 2024



Copyright: © 2024 by the authors. Licensee MDPI, Basel, Switzerland. This article is an open access article distributed under the terms and conditions of the Creative Commons Attribution (CC BY) license (<https://creativecommons.org/licenses/by/4.0/>).

Keywords: dissimilar weld; arc welding; laser beam; filler metal; dilution; weld zone; solidification mode; heat-affected zone

1. Introduction

The welding of dissimilar steels, such as those between tubes at low and high temperatures in power and process industries, allows the combination of the different properties of the two parent metals with the aim of minimizing the material cost and maximizing the joint performance. The choice of welding process and working parameters depends on physical (melting point, thermal conductivity, and thermal expansion) and metallurgical properties (microstructure, thermal stability, and the possible formation of undesirable phases).

There are different welding procedures for dissimilar metals and, of course, fusion welding is limited only to alloys with similar melting points; for a broad classification of the processes for dissimilar materials, see [1,2], in which critical factors in welding and issues regarding physical properties and metallurgical characteristics of materials are discussed. Dissimilar steel joints are usually obtained by fusion welding techniques, rather than by other ones (such as friction stir welding), mainly because the former allow full control of the composition of the final welded joint, and, therefore, of its properties. Furthermore, arc welding is a simple technology used for steel plates and tubes, whose results are particularly suitable when working “in situ” compared to other methods. Laser beam welding (LBW), although requiring complex equipment, allows the joining of thick plates or tubes in a single pass.

Recently, the progress and latest status of the selection of welding processes have been dealt with in [3], collecting and hierarchically reorganizing decision criteria and sub-criteria.

Fusion welding processes can be specifically applied to connect low-carbon or low-alloy steel components to those made of high-alloy steels, which are better suited to low- or elevated-temperature service in the adverse environments typical of petrochemical and nuclear power plants (see [4] for a review on the arc welding of dissimilar steels, and [5] for a review on the LBW of dissimilar metals). The usefulness of having the peculiar characteristic of good corrosion resistance on one side of the joint is achieved by welding at lower cost compared to the sole use of the high-alloy metal (for a summary of the common issues in the fusion welding of dissimilar steels, see the article by Ekeh et al. [6]).

In dissimilar steels, the final composition of the weld zone (WZ) will depend on that of the filler and the two parent (or base) metals. Usually, the filler metal has a different composition than the parent metals: for welding austenitic and ferritic steels, it is generally austenitic and in several cases Ni-based alloys that are used, due to their high corrosion resistance. Since the microstructure and, consequently, the mechanical properties of the weld are closely related to its composition, the dilution degree plays a fundamental role in the welding of dissimilar steels. Dilution is affected, in turn, by the process parameters, which, therefore, must be specifically determined for the welding technique adopted.

Fusion welding of thick plates of dissimilar steels can be performed in multiple passes by an electric arc or in a single pass using a highly concentrated heat source such as a laser beam. As is known, the heat input is decisive, not only for the weld composition and microstructure, but also for the width and metallurgical characteristics of the heat-affected zone (HAZ). Numerous technical solutions and much research have developed in this field, as dealt with in the article by Nabavi et al. [7], in which the authors carried out an extensive review considering several pairs of dissimilar metals, such as Al/steel, Mg/steel, or Cu/steel for the automotive industry, and how they can be welded optimally.

The objective of the present article is to outline a review specifically addressed to the scientific literature on issues related to the fusion welding of ferritic/austenitic steels. The use of the two different techniques, electric arc and laser beam, will be considered separately in two specific sections, while metallurgical topics concerning the weld zone, such as the solidification mode and phase morphology, related to dilution and the thermal field, will be debated in the Section 4.

2. Electric Arc Welding

Arc welding processes require less plant complexity than LBW ones and the results are advantageous as the equipment, cheap and portable, allows in situ joints, making them suitable for large structures. However, due to the high heat input transferred to the work pieces, the arc welding technique generally involves a large HAZ, excessive dilution, distortion of the welded parts, and a tendency to pore formation [8].

Mvola et al. [9] dealt with the general requirements for the fusion welding of dissimilar ferrous metals, focusing on the gas metal arc welding (GMAW) process, in which the filler metal is fed in the form of wire and acts as an electrode. They addressed the key issues related to the weldability of dissimilar steels, which in general concern the choice of process parameters, filler metal, and dilution ratio so that both the WZ and HAZ are suited to the foreseen service. Dilution is determined by the respective contributions to the WZ of the filler and two base metals (Figure 1); therefore, in the case of carbon or low-alloy steel joined with stainless steel, attention should be paid for a correct value, in order to prevent the risks of martensite formation in the weld as well as hot cracking because of an excess of P and S impurities when the carbon steel contribution prevails [10].

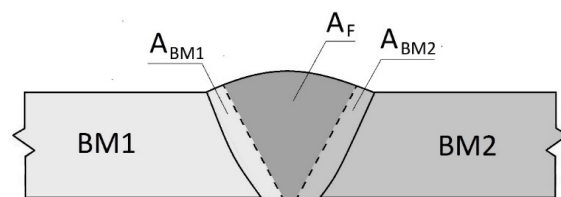


Figure 1. Schematic drawing of a weld cross-section with indication of the weld volume per unit length $A_W = A_F + A_{BM1} + A_{BM2}$ (with A_W , area of the weld cross-section; A_F , contribution of the filler metal; and A_{BM1} and A_{BM2} , contributions of the two base metals).

In [9], the authors use the Schaeffler diagram to deduce the phases in the WZ according to its composition (expressed as weighted amounts of γ -stabilizer and α -stabilizer elements); however, the updated version (the WRC1992 diagram) allows a more accurate evaluation of the residual ferrite percentage in the austenitic matrix, as will be covered in the Section 4.

The effect of welding speed on dilution, microstructure, and electrochemical corrosion was investigated in [11]: gas metal arc welding (GMAW) trials, under different welding speeds, between low-carbon steel and AISI 304 austenitic steels were carried out. ER 309L filler metal was added in the form of a consumable wire electrode, in order to compensate for Cr and Ni dilution in the molten pool. In this way, the Cr and Ni compositions in the weld joints was higher than in the two base metals and increased as the welding speed reduced (i.e., as the heat input increased). The corrosion performance of the weld also improved as the welding speed decreased.

An extensive review of the performance of dissimilar welds in an arctic environment was carried out in [12]. This article dealt with the effects of welding processes on the weld properties, considering various aspects (such as joint preparation shape, parent metals, and consumable electrode compositions), in particular with regard to the effects on low-temperature toughness.

Tungsten inert gas (TIG) welding or gas tungsten arc welding (GTAW) is widely used, especially in the case of thin sections where a filler metal is not necessary. For a general review of the employment of this process in dissimilar steel welding, see the article by Echezona et al. [13].

Shojaati and Beidokhti [14] carried out the butt welding of ferritic (AISI 409)/austenitic (AISI 304) plates (3 mm thick) in a single pass by GTAW. They investigated the effects of filler metals with different compositions: ER 310, ER316L, ER2209, and NiCr 80/20. The mechanical performance obtained with the ER316L austenitic filler metal represents a good compromise considering the lower cost.

Multi-pass welding is particular to thick components, such as boilers or furnace tubes, as it allows the deposition of the filler metal, layer by layer, into the weld groove; however, it produces at each pass a reheating of the previous passes [15] as well as dilution [16], which can affect the weld mechanical properties.

The multi-pass technique is widely used for dissimilar steels, as shown in the review previously cited [9]. Several articles have documented the effects of multi-passes on the final microstructure: in [17], the authors studied the joint between AISI 430 ferritic steel and AISI 304 austenitic steel thin plates, performed autogenously by GTAW; in [18], the joint between low-carbon steel and AISI 316 austenitic steel (using GTAW for the root pass and SMAW for the subsequent multi-passes) was investigated and compared to that produced in a single pass by SMAW.

Bahador et al. [19] investigated the effects of three different wire filler metals (ER80-Ni1, ER309L, and ER NiCrMO-3 (Inconel 625)) on the final microstructure of the welds between the structural steel A516 Gr 70 and the austenitic stainless steel AISI 316 L, produced by GTAW with pure Ar as the shielding gas. Since the plates were 12 mm thick, their edges were beveled to an angle of 45° and the multi-pass technique was adopted. Among the three different filler metals investigated, the third (Inconel 625) was found to be the most

suitable because it showed the highest tensile strength and best hardness distribution in the weld cross-section.

The effects of GTAW multi-passes and different bevel angles of the V-groove on dissimilar butt-positioned plates, made of pipeline steel (API X52) and super duplex stainless steels (SDSS 25Cr7Ni), were analyzed in [20]. Based on previous articles [21,22], the choice of welding parameters and filler metal (ER2594) arose from a compromise, taking into account how microstructure is crucial for corrosion resistance. The results given in [20] focused on the effects on corrosion behavior of the welds, showing that, with a bevel angle of 75°, slower cooling rates give rise to the microstructure best suited to reducing the corrosion rate.

In a recent article [6], the authors investigated the dissimilar joints between DSS 32205 duplex stainless steel and API 5LX60 steel, obtained by GTAW and a ERNiCrMo-3 filler metal, in order to achieve good performance for offshore applications.

The TIG process activated by a fusible flux (A-TIG) was successfully investigated by Zhang et al. [23] for welding Q245R mild steel to AISI 321 austenitic stainless steel. The surfaces of the metals to be welded were coated by a thin layer of flux, consisting of a mixture of oxides, which, by capturing electrons, improves the arc performance. It resulted in an increased weld penetration and no defects, such as gas holes, inclusions, and cracks. Consequently, the welds showed better strength and toughness than those obtained by conventional TIG welding.

Yilmaz and Tumer [24] considered the joining between the low-alloy steel AH36 and the austenitic stainless steel AISI 304 L with flux-cored arc welding (FCAW). This process uses a consumable tubular electrode which continuously feeds the weld, whose core produces a flux of liquid slag protecting the melting pool. The authors investigated the effects of the shielding gas composition, observing that the impact performance of the weldment decreases if the CO₂ content increases; furthermore, it also involves an increase in the austenitic volume and thus a reduction in the δ -ferrite percentage in the WZ.

In shielded metal arc welding (SMAW), the electrode plays a significant role in weld quality. In fact, in addition to protecting the filler metals, the decomposition of the coating produces slag, which acts at the interface with the molten pool, and leads to gaseous protection from oxidation [25]. The article by Bhandari et al. [26] aimed at developing a SMAW process for joining dissimilar plates (SA516 and AISI304L) using coated electrodes. Pratiwi et al. recently published [27] an experimental study with the aim of optimizing the SMAW process parameters for welding ASTM A36 mild steel to AISI 316 austenitic steel.

The submerged arc welding process (SAW) was also investigated: a layer of 309L stainless steel was deposited on a plate of 18MND5 low-alloy steel (similar to ASTM A533 grade B or DIN 1.6308), [28]. A granular fusible flux of silica, fluorides, and other oxides protected the molten pool and the arc zone from atmospheric contamination. In this process, only one layer was deposited so that its microstructure, which was not modified by any thermal effects due to subsequent passes, allowed the documentation of the solidification mode of the austenitic weld bead.

Any misalignments of the electric arc with respect to the axis of the joint can lead to an asymmetric contribution by the two base metals giving rise to an incorrect dilution. In some cases, the buttering technique at the carbon steel side (Figure 2), with the use of a proper composition of the filler metal, is recommended to compensate for the differences in composition between the two metals to be welded. However, it is always necessary to consider the effects of all the parameters that characterize the welding process on which dilution depends.

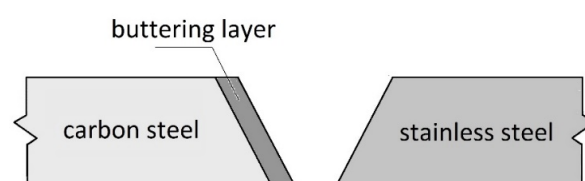


Figure 2. Schematic drawing of two butt-positioned plates with the buttering layer at the carbon steel side.

References [26,29,30] can be cited as examples of buttering techniques. In [26], to compensate dilution, SS309L electrodes were used for depositing a layer rich of Ni and Cr on the carbon steel edge; subsequently, SS308L electrodes were used to join two dissimilar plates (SA 516 and AISI 304L) by SMAW. Mechanical tests showed that the ultimate tensile strength of the welds increased due to the individual effects of the TiO_2 , SiO_2 , and CaF_2 present in the electrodes' coatings; in contrast, the interaction effects of the binary mixtures $\text{CaO}\cdot\text{SiO}_2$, $\text{CaO}\cdot\text{CaF}_2$, and $\text{SiO}_2\cdot\text{CaF}_2$ caused a significant decrease.

In [29], the buttering technique was used in the GTAW of two dissimilar plates (A508 Grade 3 and AISI 304 L), which were butt-positioned and prepared with a conventional V groove. The low-alloy steel side was buttered by an ERNiCr-3 filler wire; however, islands of martensite and complex alloy carbides were observed near the fusion line boundary at the low-alloy steel side. The authors also investigated GTAW between the same plates, butt-prepared with a narrow gap and without buttering. This preparation required less heat input during welding; regarding the metallurgical and mechanical characteristics, the weldment showed better performance than that obtained with the buttering preparation.

More recently, Asadollahi et al. [30] have investigated the effects of three different filler metals (ER308L, ER309L, and ERNiCr3) in the GTAW of the dissimilar plates API 5L X65 and AISI 304 L (10 mm thick). Before welding, the ferritic steel edge was prepared with a buttering layer (6 mm thick), through GTAW passes with an ERNiCr3 filler wire. First, if compared to non-buttered welds, the results of the metallographic investigations demonstrated that buttering hinders the formation of a brittle martensitic/bainitic layer at the fusion line. The results of mechanical tests showed that the best properties were achieved in the sample welded with the ERNiCr3 filler metal.

3. Laser Beam Welding

Nowadays, LBW has also become widespread for dissimilar metals due to the high degree of automation and accurate energy control, mainly by means of a CO_2 or Nd:YAG laser apparatus; moreover, fiber laser technology has only recently caught on [31] for its beneficial impact on beam guidance. The high level of energy concentrated in a small volume allows it to work at a higher welding speed than arc welding, obtaining with a single pass narrow and deep joints in thick steel plates. Another advantage over conventional arc welding is the small size and accuracy of the beam spot that give rise to the reduced sizes of both the WZ and HAZ. In this regard, the beneficial effects on the mechanical properties of both rapid solidification in the WZ and small width of the HAZ were investigated in mild steel/austenitic steel joints produced by LBW [32].

Even if the formation of embrittling intermetallic compounds can occur, this problem is smaller in LBW than in conventional arc welding [2]. However, due to the rapid solidification of the molten pool, LBW generally shows a high tendency to solidification cracking, which can be controlled by a careful selection of the filler metal and the welding parameters, as will be debated in the Section 4.

The high production rate makes LBW suitable for high productivity in series; furthermore, the investment resources in laser equipment are well compensated, due to the good performances and cost savings achieved for different pairs of dissimilar metals [5].

Regarding applications in the field of dissimilar materials, LBW has been considered in power generation systems as well as in the automotive industry which requires appropriate methods for joining steels and light alloys. In fact, the small size of the weld pool reduces diffusion and mixing between the two materials compared to traditional electric arc techniques, as amply demonstrated by the scientific literature on this subject [33,34].

With a suitable choice of welding parameters, the laser beam produces a narrow and deep plasma zone, the so-called "keyhole", which in turn solidifies as a narrow weld bead with a reduced width of the HAZ. Furthermore, the keyhole mode produces rapid cooling and, consequently, reduces the exchanges of alloying elements by diffusion between the WZ and parent metals. In these conditions, AISI 304 stainless steel thick plates, 12 mm thick, can be welded in a single pass without any filler metal [35].

In recent years, LBW has been utilized for joining ferritic/austenitic dissimilar steels and some researchers have addressed their efforts to butt-joining thin sheets without filler metals: AISI 1010 to AISI 321 in [36], AISI 1010 to AISI 304L in [37], 9Cr-1Mo-V-Nb to 316 L(N) in [38], and S235JR to AISI 316L in [39]. However, in the absence of a filler metal with a composition such as to compensate for the absence of alloying elements in carbon steel, dangerous martensitic microstructures have been observed in the welds, due to carbon diffusion (see references [40,41]), which can be overcome by post-welding heat treatments [42,43].

In [40], Hamada et al. performed an autogenous LBW of Docol S355 to AISI 201 medium-Mn stainless steel. The presence of martensitic structures was highlighted in the welds and, therefore, post-welding heat treatment was necessary to homogenize the microstructure, relieve residual stress, and, therefore, improve mechanical performances.

Recently, in [41] the authors investigated the effects of two different heat inputs in LBW between S355 low-alloy steel and AISI 316 austenitic stainless steel. Two dissimilar plates (5 mm thick) were butt-positioned and autogenously welded with a constant laser beam power at two different welding speeds. Metallographic investigation showed in the WZ a martensitic microstructure with 5% austenite that became fully martensitic when the heat input increased (i.e., the welding speed decreased). Higher values of micro-indentation hardness were measured in the case of a fully martensitic microstructure.

The potential of post-welding heat treatments has also been considered in the literature: Prabakaran and Kannan, using process parameters optimized in a previous work [42], performed LBW between AISI 1018 and AISI 316 thin sheets, in a single pass and without filler metal, and then carried out a post-welding heat treatment at 960 °C [43]. In this way, a microstructure of pure martensite with no carbide precipitates was obtained in the WZ, resulting in an improved mechanical strength.

Liu et al. [44] considered autogenous LBW between AH36 and AISI 304 thin sheets (3 mm thick) and showed, through metallographic investigation and numerical simulation, that changes in the laser beam offset (Figure 3) affect the melt flowing, the shapes of fusion boundaries, and, consequently, the final chemical composition of the weld and its microstructure.

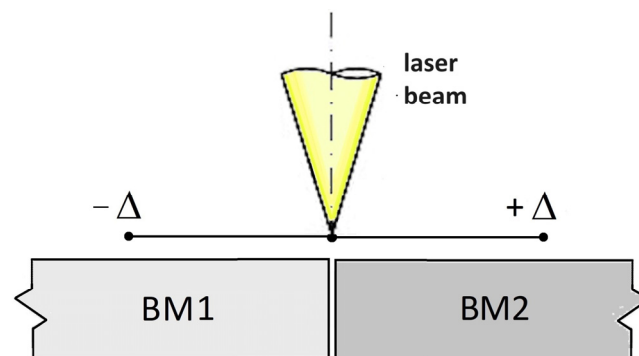


Figure 3. Sketch of the laser beam offset considered for research purposes ($\Delta = 0.5$ mm [44]).

The issues related to the thinness of the laser beam, which entails very strict requirements on machining and the assembly of a workpiece, can be overcome with hybrid laser-arc welding (Figure 4). Some authors have explored the synergic effects of a welding torch and a laser beam which travel a few millimeters of distance along the same axis. The results given in the literature (see for example Li et al. [45] for welding thick plates of mild steel, or Spina et al. [46] for welding Mn steel to dual-phase steel) can be considered preparatory for applications in welding ferritic/austenitic dissimilar steels. In this regard, the work of Zhang et al. [47] is exemplifying, as it demonstrates how an acceptable 20 mm thick weld between dissimilar EH36 mild steel and 316L austenitic steel can be obtained by optimizing the welding parameters of a narrow-gap hybrid laser-arc welding process.

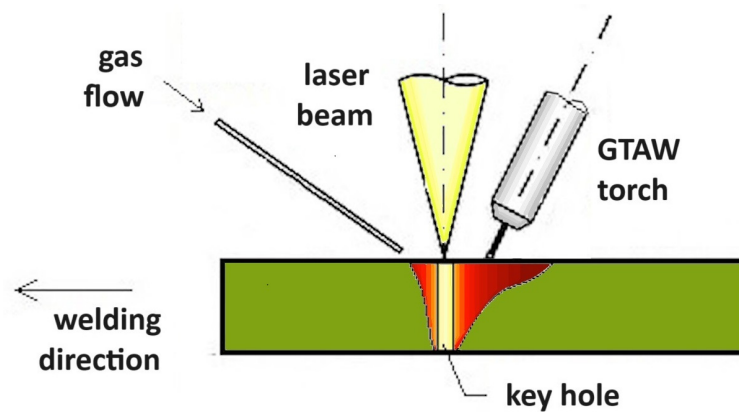


Figure 4. Sketch of hybrid laser–arc welding setup [48].

It is known that in LBW processes the use of a filler wire entails stringent requirements for positioning [49]. On the other hand, a laser beam allows for the deep autogenous welding of thick plates; however, in the case of dissimilar metals, the use of an appropriate filler metal is crucial to compensate for dilution and achieve a good weld performance.

An alternative to the filler wire could be the addition of consumable inserts, interposed between the edges of two butt-positioned plates. This solution was adopted in [48] for a particular case of dissimilar ferritic/austenitic steels: as shown in Figure 5, two plates of carbon steel clad with austenitic steel (total thickness of 10 mm) were LBW-ed in a single pass, achieving good results with a suitable choice of welding parameters (this procedure is very advantageous when compared to the traditional multi-pass arc welding process with a wire filler metal used for clad steel plates [50]).

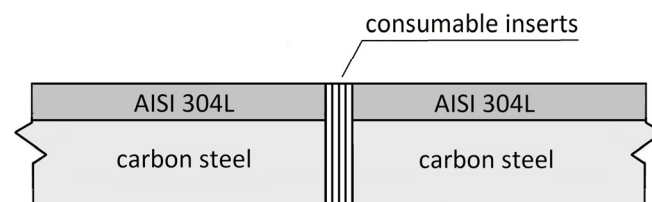


Figure 5. Setup for the LBW of clad steels with interposed consumable inserts [48].

Fiber laser technology has only recently caught on for beams of outstanding optical quality and precise welding action [31]. High-power fiber lasers allow a beam to be split into multiple beams (each one with an intensity sufficient to work in the keyhole mode), which can be shaped in a pre-defined pattern of multiple spots to reproduce the actual joint configuration.

Although there are references in the literature to the multi-beam welding between stainless steel or between carbon steel and aluminum sheets, it is worth considering that this technique could also be useful for joining dissimilar steels. In [51], the authors demonstrated that it is possible to produce a bead with a rectangular cross-section by correctly choosing the spot configuration and the working parameters. For a row of multiple spots, they obtained an equal penetration depth if the edge spots had 5%–10% more power than the center spots. Beam splitting, produced by a high-power fiber laser apparatus, was used to butt-weld four stainless steel sheets placed in a complex geometry [52]. The pattern utilized for the multiple beams was side-by-side, characterized by three spots for each of the three joints to be welded. Furthermore, Cui et al. successfully performed LBW of steel/Al lapped joints by means of a dual-beam with a side-by-side configuration (Figure 6) [53]. These results seem encouraging for the use of the multiple-spot technique in welding dissimilar steels.

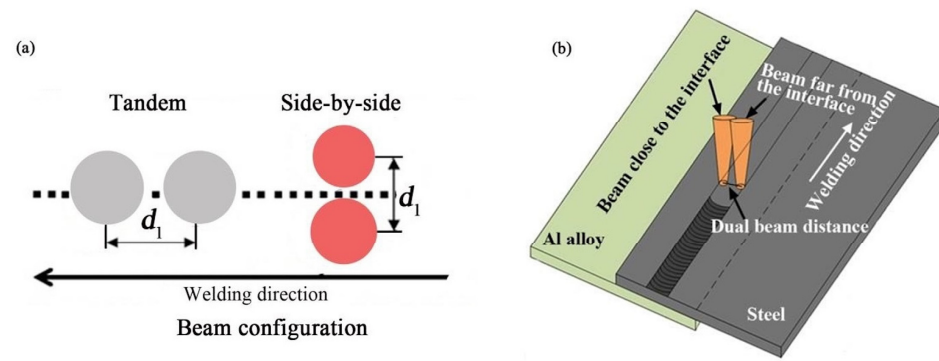


Figure 6. (a) Tandem and side-by-side configurations; (b) setup of the side-by-side configuration (reproduced from [53]).

4. Discussion

Physical and mechanical properties are not the same in the weld and parent metals. For example, the linear thermal expansion coefficient λ ($^{\circ}\text{C}^{-1}$) varies from about $13 \cdot 10^{-6}$ for carbon steel to $17 \cdot 10^{-6}$ for AISI 304 austenitic steel and $10 \cdot 10^{-6}$ for AISI 430 ferritic steel; and heat conductivity k ($\text{W}/(^{\circ}\text{C} \cdot \text{m})$) from 45 for carbon steel to 16 for AISI 304 and 25 for AISI 430. The difference in the coefficients of thermal expansion between ferritic and austenitic steels gives rise to distortions or, when prevented, to thermal stresses, as shown by the numerical simulation carried out in [54,55]; moreover, recent experimental measurements and numerical simulations have been performed investigating the effects of cooling and heating cycles during service [56].

Anyhow, in dissimilar welding it is more difficult to control the composition of the molten zone, which plays a fundamental role in determining the microstructure and mechanical properties and, therefore, the weldability of the parent metals involved. Attention must be paid to the presence of elements forming carbides or intermetallic compounds, which are detrimental to mechanical performance [57] and to corrosion resistance [58]. In particular, when welding dissimilar ferritic/austenitic steels, carbon steel of low quality could provide elements, such as sulfur and phosphorus, which segregate at the boundaries of the austenitic dendrites in the WZ, generating low-melting eutectic phases and giving rise to solidification cracks [59,60].

To avoid these risks, the WZ composition must be balanced by the addition of an adequate filler metal, whose effects depend on the dilution ratio. The following relationships give the dilution ratios in respect to the filler metal (d_F) and to the two base metals (d_{BM1} and d_{BM2}):

$$d_F = A_F / (A_F + A_{BM1} + A_{BM2}), \tag{1}$$

$$d_{BM1} = (A_{BM1}) / (A_F + A_{BM1} + A_{BM2}), \tag{2}$$

$$d_{BM2} = (A_{BM2}) / (A_F + A_{BM1} + A_{BM2}), \tag{3}$$

where A_F , A_{BM1} , and A_{BM2} represent the volumetric quantities of the filler metal and the two base metals, respectively, which are reduced by one dimension into area terms under the assumption that the cross-sectional areas do not vary along the weld bead length [10].

Once the dilution values are known, the WZ composition results from a weighted mass balance. Then, its microstructure can be estimated, based on Cr_{eq} and Ni_{eq} compositions, through the Schaffler diagram (based on the equivalent compositions expressed as percentages by weight: $\text{Cr}_{\text{eq}} = \text{Cr} + 1.5 \cdot \text{Si} + \text{Mo} + 0.5 \cdot \text{Nb}$ and $\text{Ni}_{\text{eq}} = \text{Ni} + 30 \cdot \text{C} + 0.5 \cdot \text{Mn}$), or by means of the more recent development, the WRC 1992 diagram ($\text{Cr}_{\text{eq}} = \text{Cr} + \text{Mo} + 0.7 \cdot \text{Nb}$ and $\text{Ni}_{\text{eq}} = \text{Ni} + 35 \cdot \text{C} + 20 \cdot \text{N} + 0.25 \cdot \text{Cu}$). They are currently used by many researchers (see [9,61,62] for the Schaffler diagram and [63–65] for the WRC 1992 diagram).

When ferritic/austenitic dissimilar steels are welded without filler metals, dilution in the WZ gives rise to compositions within the martensitic range (Figure 7).

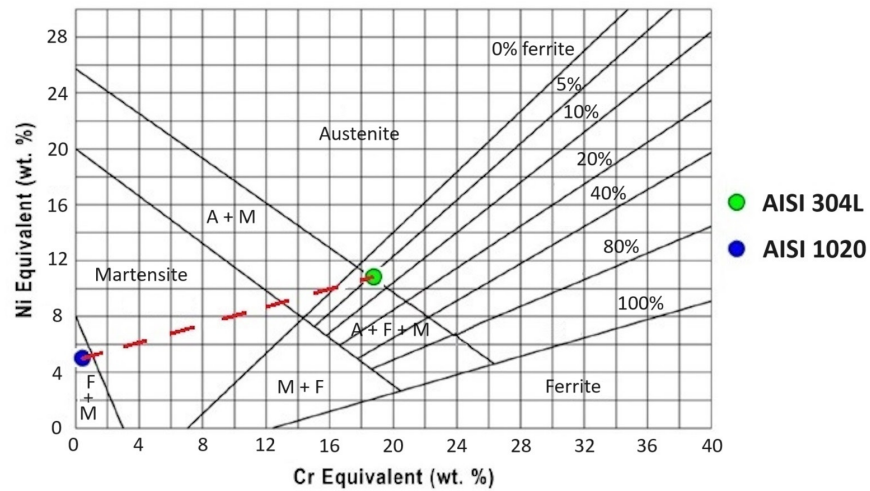


Figure 7. Schaeffler diagram (adapted from [62]): the red dashed line represents the composition range of the WZ in relation to the dilution ratio.

In the case of dissimilar welding between AISI 1020 and AISI 304L thin sheets without filler metal (Figure 8), Scutelnicu et al. [37] documented the formation of a hard, martensitic microstructure in the WZ, as shown in Figure 8 by the results of Vickers hardness measurements, performed along a traverse on the joint cross-section from the CS-side (AISI 1020 mild steel side) to the SS-side (AISI 304L austenitic steel side). These results are confirmed by the SEM images in Figure 9, which show the presence of martensite in the WZ.

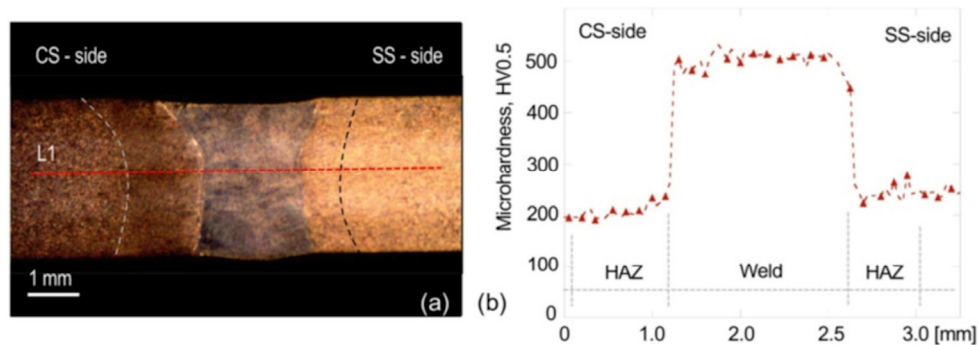


Figure 8. Hardness analysis. (a) Location of the microhardness imprint line L1 on the joint section; (b) microhardness profile along the analyzed line (reproduced from [37]).

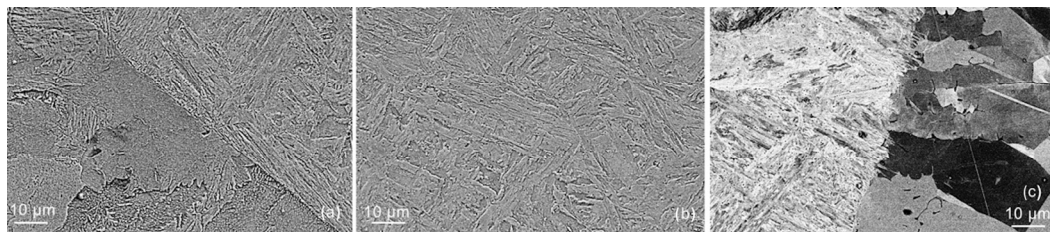


Figure 9. SEM micrograph across the WZ: (a) CS-side and the WZ (on the right), (b) WZ with martensitic microstructure, and (c) WZ and SS-side (on the left). Reproduced from [37].

For compositions in the ferritic austenitic field, solidification takes place following the modes listed in Table 1, according to [66–68], even if some authors report slightly different limit values [7 Nabavi].

Table 1. Solidification modes of stainless steels.

Composition Ranges	Solidification Modes	Sequence of Transformations
$C_{req}/Ni_{eq} > 2.0$	F (ferritic)	$L \rightarrow L + \delta \rightarrow \delta$
$1.5 < C_{req}/Ni_{eq} < 2.0$	FA (ferritic-austenitic)	$L \rightarrow L + \delta \rightarrow L + \delta + \gamma \rightarrow \delta + \gamma$
$1.37 < C_{req}/Ni_{eq} < 1.5$	AF (austenitic-ferritic)	$L \rightarrow L + \gamma \rightarrow L + \delta + \gamma \rightarrow \gamma + \delta$
$C_{req}/Ni_{eq} < 1.37$	A (austenitic)	$L \rightarrow L + \gamma \rightarrow \gamma$

In general, the austenitic microstructure tends to be less susceptible to solidification cracking when the solidification mode is FA, characterized by primary δ -ferrite, while the other solidification modes show worse behavior. The main reason is the presence of ferritic–austenitic boundaries at the solidification end, which resist wetting by liquid films containing low-melting phases responsible for hot cracking [69]. In this case, about 5% of retained primary ferrite is usually considered as a requirement for an austenitic weld to avoid solidification cracking [70].

For compositions such as that of AISI 309L (usually utilized as filler metal), the final solidification microstructure contains retained primary δ -ferrite with a vermicular/skeletal morphology, which occupies the core of the austenitic dendrites, coming in turn from the transformation of ferrite into austenite after solidification (FA mode). The skeletal morphology is favored for a low cooling rate (high heat input) [71]. Indeed, the lathy columnar morphology is favored for by a higher cooling rate [72]. Figure 10 shows a comparison of these two morphologies, observed after different passes of arc welding [68].

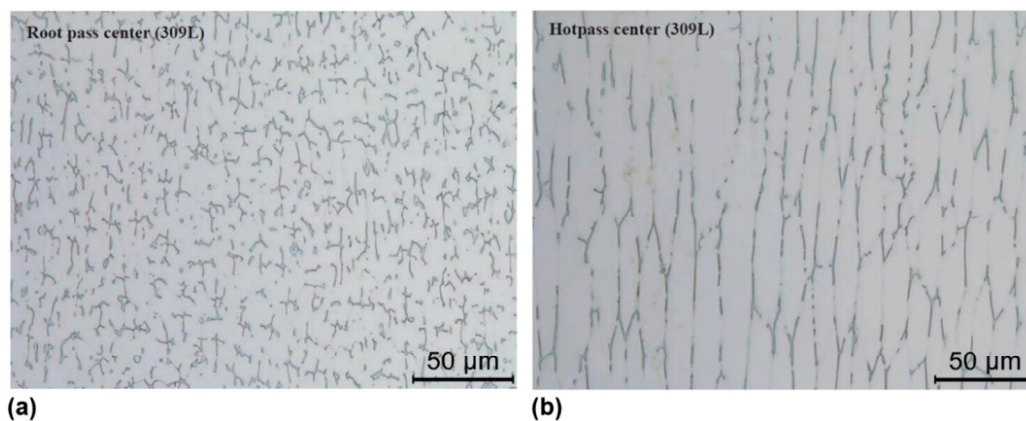


Figure 10. Residual primary ferrite (dark phase) in austenitic matrix: (a) vermicular morphology, (b) columnar morphology. Reproduced from [68].

Zhou et al. [73] demonstrated that, in an austenitic WZ, the presence of residual ferrite with a skeletal morphology also prevents hydrogen embrittlement. However, concentrations of ferrite of around 10% and above promote selective attack by some corrosive media; moreover, when working temperatures are in the 550–900 °C range, primary ferrite could decompose into carbides and phases detrimental to mechanical properties, such as ductility, impact toughness, and creep strength, as well as corrosion resistance [74]. For these reasons, its content in the weld metal should be limited [75].

The content and morphology of residual ferrite are affected by the welding heat input [73]. For high heat input, and consequently slow cooling rate, the solidification time gets longer and thus the initial content of ferrite is high; however, the duration of the transformation $\delta \rightarrow \gamma$ is prolonged, leading to a possible reduction in the primary ferrite content, caused by increased formation of austenite; instead, if the heat input is lowered, the cooling rate increases, resulting in a possible increase in the ferrite content. The balance between ferrite formation and its transformation into austenite leads to competing effects, as confirmed by experimental observations: some authors [24,71] agree with the described trend, while other authors have detected the opposite [76,77].

However, if cooling rate exceeds a limit value, the FA mode could be completely cancelled out and the austenitic molten pool could solidify as primary austenite, instead of as primary ferrite [78].

Regarding the morphological aspects, the ratio between the temperature gradient (G) and solidification rate (R) represents a useful parameter. The G/R value is high close to the fusion line, where the solidification is planar/cellular, while it decreases approaching the weld centerline where an equiaxed microstructure occurs under a sufficient undercooling [79]. The presence of alloying elements favors the formation of the dendritic morphology, as shown for three representative metals in Figure 11, taken from [68]. Note that X65C carbon steel, being low in alloying elements, undergoes planar solidification over a wide range of G/R values.

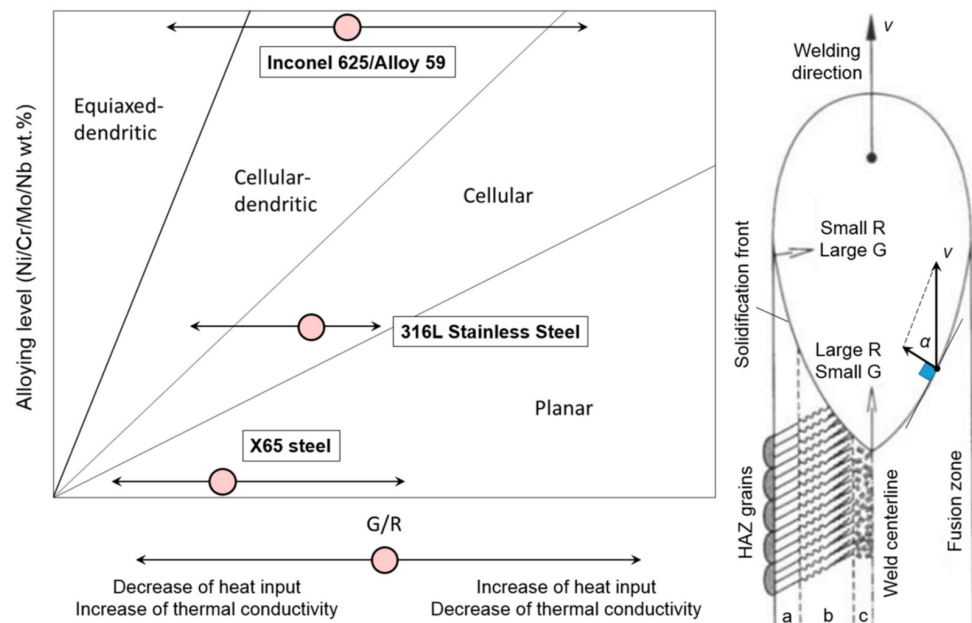


Figure 11. On the left, solidification modes for three representative metals, according to the ratio G/R and alloying elements content; on the right, sketch of the solidification morphology around the molten pool: (a) cellular, (b) cellular-dendritic, and (c) equiaxed-dendritic solidification mode. Reproduced from [68].

For an in-depth microstructural study of a carbon steel/austenitic steel weld, see the reference [28] already cited in the arc welding section. In this article, the authors published an optical micrograph of the weld cross-section, which shows that on the carbon steel side the original bainitic microstructure becomes martensitic in the HAZ, followed on the weld side by a narrow layer of martensite, then by a fully austenitic zone and finally by the typical microstructure of the austenitic stainless steel with 18% Cr and 9% Ni, characterized by a γ matrix with residual ferrite (Figure 12a). These observations are confirmed by the composition profiles of Fe, Ni, and Cr, obtained with EDS measurements and shown in Figure 12b: starting from the HAZ, first the profiles are flat, then sharp gradients of the alloying elements characterize the transition towards the homogeneous mixing in the molten pool, of which the author determined the proportions 20% base metal and 80% filler metal.

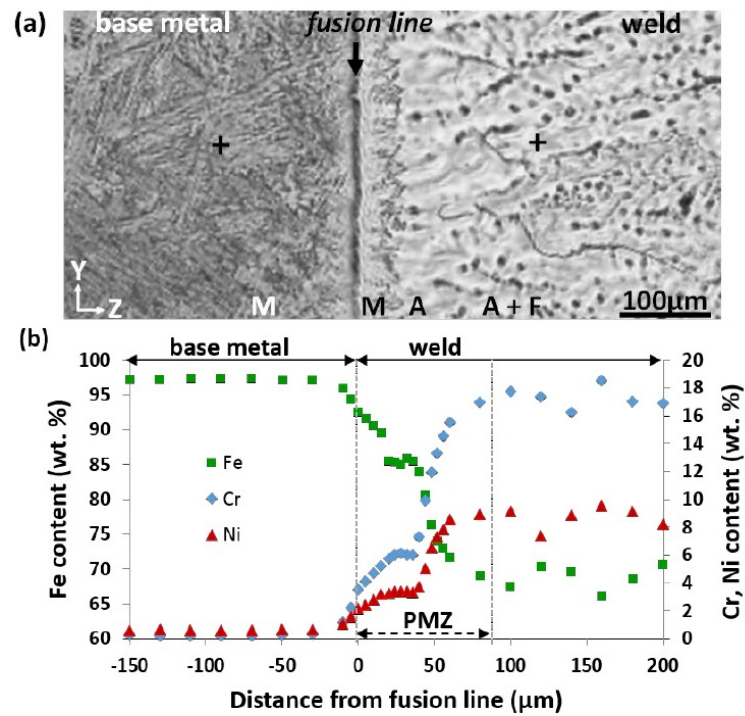


Figure 12. Weld cross-section: carbon steel (base metal) and austenitic steel (weld): (a) optical micrograph with indication of microstructure (M martensite, A austenite, and A + F austenite and ferrite); (b) composition profiles of Fe, Ni, and Cr vs. the distance from the fusion line. Reproduced from [28].

In this regard, starting from the fusion line, Mas et al. [28] documented the following sequence of solidification: cellular A mode (γ_1), cellular AF mode (γ_1, δ), and dendritic FA mode ($\delta_1, \gamma_2, \gamma_2$) with evidence of skeletal primary ferrite (Figure 13).

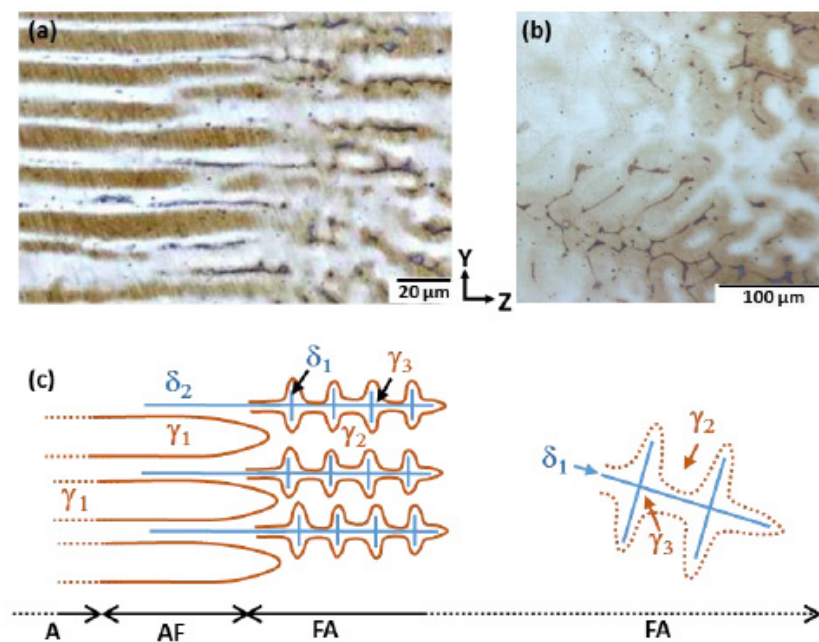


Figure 13. Evolution of the solidification mode of the weld (austenite in dark/light brown and ferrite in black): (a) microstructure close to the fusion line; (b) microstructure far from the fusion line; and (c) evolution of the solidification mode. Reproduced from [28].

In general, welding speed has an important effect on cooling rates as investigated in the literature by finite elements methods [80], using a commercial software [81], or by a new analytical model experimentally fitted on the weld cross-section contour, which was presented in [82] and validated in [83]. It would be appropriate to find articles that specifically deal with the effects of welding speed on cooling rates in welds between dissimilar steels. Unfortunately, there is a lack of articles on this topic. In this regard, the prediction of cooling rates produced during LBW of two thick AISI 304L plates, with AWS 309L inserts as filler material, provided useful indications for welding dissimilar ferritic/austenitic steels [64]; in fact, although the cooling rates could influence the ferrite—austenite transformations, for the welding conditions considered, they do not reach values that affect the expected percentage of primary ferrite in the weld, according to the WRC 1992 diagram.

The effects of re-heating due to multi-passes on the WZ and HAZ of the joint between low-carbon steel and AISI 316 steel was studied in [18]. The authors documented some differences in the microstructure between single-pass and multi-pass welding. In the first case, the WZ microstructure is characterized by the transformation from cellular to columnar and equiaxed dendrites, while, in the second case, the columnar dendrites are extended from the fusion line of one weld pass towards the subsequent one. Because of the recrystallization processes generated by the heat input of the various passes, multi-pass welding showed grain refinement and higher hardness on the carbon steel side than single pass welding.

Regarding the HAZ, on the austenitic side the occurrence of conditions that favor sensitization to intergranular corrosion must be considered. This phenomenon is due to Cr atom depletion near the austenitic grain boundaries, caused by Cr-carbide precipitation during welding within the range 400–800 °C (for a review on this topic see [84]). At a given temperature, the higher the carbon content, the shorter the precipitation time: for example, in austenitic steel containing 0.056% carbon, at 700 °C, 7 min is needed for sensitization [75]. Carbide precipitation is easily detectable, as it produces increases in hardness, and can be recovered through heat treatment at the homogenizing temperature in the range 1000–1100 °C, followed by a reduction in hardness [85].

During the LBW of AISI 304 thick plates performed in [64], the conditions favorable for sensitizing were not reached, because the exposure time within the critical temperature interval was only a few seconds, as shown by the simulation of the thermal fields.

Conversely, Dae et al. [86] carried out multi-passes of GTAW on butt-positioned thick plates of dissimilar ASTM 335 P92 martensitic steel/AISI 304 austenitic steel, using Alloy 82 as the filler metal. Their work was aimed at developing a model that can accurately predict the zone with the most serious degree of sensitizing: the results indicated that sensitization mainly occurred on the austenitic side, in the lower half of the joint at a distance of approximately 7.5 mm from the WZ boundary.

On the ferritic side of dissimilar steels, one is likely to encounter a microstructure with high hardness, such as martensite and bainite, depending on the process setup and the adopted welding parameters, which determine the heating in the austenitic field and the subsequent rapid cooling [87]. However, it should be considered that ferritic steels have a higher carbon content than austenitic steels, in which carbon concentration is usually limited to avoid sensitizing phenomena. Therefore, the carbon gradient favors the diffusion of this element towards the austenitic side; furthermore, the solubility of this element is higher in austenite than in ferrite, while the diffusion coefficient is much higher in ferrite. These factors together generate a strong carbon diffusion from the ferritic base steel to the austenitic WZ, resulting in carbon depletion on the ferritic side near the fusion line and a consequent local reduction in hardness, which can affect a zone about 50–100 µm wide [88].

A difference in chemical composition between base and weld metals can be created intentionally, as performed in [89] by choosing a CN 23/12 Mo-A austenitic filler metal for GTAW two ASTM A335 P91 martensitic steel plates. The welding trial was performed in a single pass to eliminate the consequence of re-heating. In this way, the authors

investigated the effects of the heat input and pre-welding thermal treatments on the width of the decarburized layer. In [90], the same ASTM A335 P91 martensitic steel was joined to AISI 304L austenitic steel by multi-passes of GTAW using two different filler metals (309L-16L or ERNiCr-3). The weldability of this pair of dissimilar steels was studied by microstructural investigations of the weld metal and the HAZ, as well as mechanical tests, determining that ERNiCr-3 is the preferred filler. Moreover, the authors ascertained that the weld microstructure consisted of austenitic dendrites with a minor fraction of ferrite in the interdendritic spaces.

5. Conclusions and Future Directions

Arc welding and LBW processes are currently used for joining dissimilar steels. Progress in this field has developed over the last 20 years, as highlighted by the vast scientific production in the literature. The majority of the articles examined (50/90) date back to the last five years (Figure 14), demonstrating that the interest in this topic remains alive.

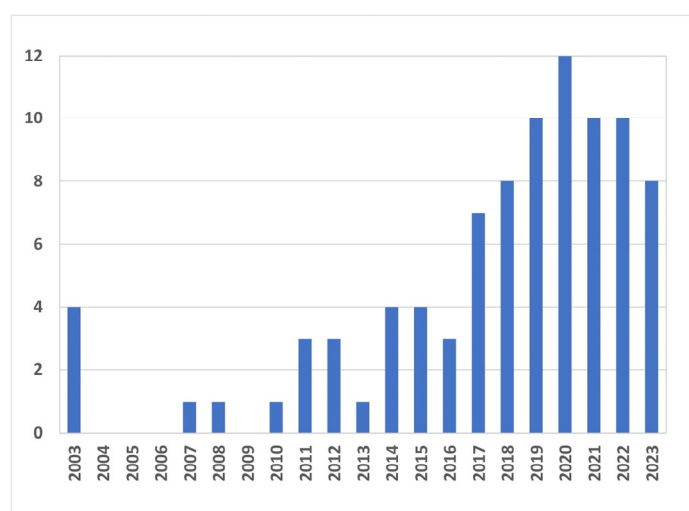


Figure 14. Temporal distribution of the articles examined in the current review.

Many researchers have directed their efforts to setting up a fusion welding process which allows full control of the composition of the WZ and optimizes the working parameters. In fact, when welding dissimilar steels, the choice of parameters is crucial, since dilution, on which depends the weld composition, is affected by the heat input.

Different arc welding techniques, such as GTAW, GMAW, FCAW, SMAW, or SAW, have been objects of research. Each of them has been analyzed by the authors for specific purposes and this has led to different evaluations, regarding both the process setup and the mechanical and metallurgical characterization of the welds.

LBW offers the possibility of welding thick plates in a single pass, thus avoiding the effect of re-heating between one pass and another. Even if LBW requires greater equipment complexity than arc welding, it has proven to be largely advantageous for the quality of welds, due to the high concentration of energy and the automatism of the welding system which allows better control of the working parameters. In this way, it is easier to limit any misalignments that can alter the degree of dilution in the weld, although the thinness of the laser beam entails very strict requirements in the machining and assembly of the workpiece, which can be overcome by hybrid laser–arc welding.

With regard to WZ metallurgy, the discussion dealt with the following issues:

- Evaluation of the WZ composition considering the effect of dilution between filler and parent metals.
- Choice of the filler metal for achieving an appropriate composition of the WZ.
- Prediction of the WZ microstructure based on its composition (Schaeffler and WRC 1992 diagrams).

- Solidification mode of the WZ in order to achieve the advantageous presence of a small content of residual primary ferrite in an austenitic matrix.
- The influence of alloying elements and welding parameters on the amount and morphology of residual delta ferrite.
- Possible formation of martensite in the case of autogenous welding.
- Diffusion of alloying elements at the interface of parent metal/WZ.
- Microstructural inhomogeneity due to reheating.

The differences in composition between the two different base metals need to be balanced by a proper composition of the filler metal, with the purpose of obtaining in the weld an austenitic microstructure with a small amount of residual δ -ferrite, which is the best condition to prevent hot cracking.

Although many articles have been published and cited in this paper, several topics (such as solidification modes, diffusion, and solid phase transformations) have been covered generically for austenitic stainless steel, so the metallurgy of the WZ is still worthy of further investigations aimed at the specific case of welding between ferritic and austenitic steels.

Another important issue to consider is the simulation of the thermal fields as a function of the process parameters. This would allow researchers to make metallurgical and mechanical predictions about the generation of residual stresses as well.

This is not to mention the improvement of laser welding processes—for example, with the use of consumable inserts as a filler material or with the refinement of spot welding by fiber laser. Considering the advantages of the multi-spot technique, the development of double laser systems, with an up and down setup, could be also desirable for welding very thick plates in a single pass.

Author Contributions: Conceptualization, F.G., S.M., C.S. and A.S.; methodology, F.G., S.M., C.S. and A.S.; investigation, F.G., S.M., C.S. and A.S.; data curation, F.G., S.M., C.S. and A.S.; writing—original draft preparation F.G., S.M., C.S. and A.S.; writing—review and editing, F.G., S.M., C.S. and A.S.; visualization, F.G., S.M., C.S. and A.S.; supervision, F.G., S.M. and A.S. All authors have read and agreed to the published version of the manuscript.

Funding: This research received no external funding.

Data Availability Statement: No new data were created; therefore, data sharing is not applicable to this article.

Conflicts of Interest: The authors declare no conflicts of interest.

References

1. Kah, P.; Shrestha, M.; Martikainen, J. Trends in joining dissimilar metals by welding. *Appl. Mech. Mater.* **2014**, *440*, 269–276. [[CrossRef](#)]
2. Martinsen, K.; Hu, S.J.; Carlson, B.E. Joining of dissimilar materials CIRP Annals—Manufacturing. *Technology* **2015**, *64*, 679–699. [[CrossRef](#)]
3. Soltan, H.; Omar, M. A roadmap for selection of metal welding process: A review and proposals. *Weld. World* **2022**, *66*, 2639–2675. [[CrossRef](#)]
4. Maruyama, T. Arc welding technology for dissimilar joints. *Weld. Int.* **2003**, *17*, 276–281. [[CrossRef](#)]
5. Boumerzoug, Z. A review: Welding by laser beam of dissimilar metals. *Asp. Min. Min. Sci.* **2021**, *8*, 916–920. [[CrossRef](#)]
6. Ekeh, T.D.; Lawal, F.T.; Osoba, L.O.; Amuda, M.O.H. Microstructure and mechanical properties of dissimilar welds of duplex and API steel for offshore applications. *Int. J. Mater. Technol. Innov.* **2023**, *3*, 80–91. [[CrossRef](#)]
7. Nabavi, S.F.; Farshidianfar, A.; Dalir, H. A comprehensive review on recent laser beam welding process: Geometrical, metallurgical, and mechanical characteristic modeling. *Int. J. Adv. Manuf. Technol.* **2023**, *129*, 4781–4828. [[CrossRef](#)]
8. Abioye, T.E.; Olugbade, T.O.; Ogedengbe, T.I. Welding of dissimilar metals using gas metal arc and laser welding techniques: A review. *J. Emerg. Trends Eng. Appl. Sci.* **2017**, *8*, 225–228.
9. Mvola, B.; Kah, P.; Martikainen, J. Dissimilar ferrous metal welding using advanced gas metal arc welding processes. *Rev. Adv. Mater. Sci.* **2014**, *38*, 125–137.
10. DuPont, J.N. Dilution in fusion welding. In *Metals Handbook*, 1st ed.; Lienert, T.J., Babu, S.S., Siewert, T.A., Acoff, V.L., Eds.; ASM: Materials Park, OH, USA, 2011; Volume 06A, pp. 115–121.

11. Abioye, T.E.; Ariwoola, O.E.; Ogedengbe, T.I.; Farayibi, P.K.; Gbadeyan, O.O. Effects of welding speed on the microstructure and corrosion behavior of dissimilar gas metal arc weld joints of AISI 304 stainless steel and low carbon steel. *Mater. Today Proc.* **2019**, *17*, 871–877. [[CrossRef](#)]
12. Mvola, B.; Kah, P.; Martikainen, J.; Suoranta, R. Dissimilar welded joints operating in sub-zero temperature environment. *Int. J. Adv. Manuf. Technol.* **2016**, *87*, 3619–3635. [[CrossRef](#)]
13. Echezona, N.; Akinlabi, S.A.; Jen, T.C.; Fatoba, O.S.; Hassan, S.; Akinlabi, E.T. Tig welding of dissimilar steel: A review. In *Advances in Manufacturing Engineering, Lecture Notes in Mechanical Engineering*; Awang, M., Emamian, S.S., Eds.; Springer Nature: Singapore, 2021. [[CrossRef](#)]
14. Shojaati, M.; Beidokhti, B. Characterization of AISI 304/AISI 409 stainless steel joints using different filler materials. *Constr. Build. Mater.* **2017**, *147*, 608–615. [[CrossRef](#)]
15. Sun, Y.L.; Obasi, G.; Hamelin, C.J.; Vasileiou, A.N.; Flinta, T.F.; Francis, J.A.; Smith, M.C. Characterization and modelling of tempering during multi-pass welding. *J. Mater. Process. Tech.* **2019**, *270*, 118–131. [[CrossRef](#)]
16. Sun, Y.L.; Hamelin, C.J.; Vasileiou, A.N.; Xiong, Q.; Flint, T.F.; Obasi, G.; Francis, J.A.; Smith, M.C. Effects of dilution on the hardness and residual stresses in multipass steel weldments. *Int. J. Press. Vessel. Pip.* **2020**, *187*, 104154. [[CrossRef](#)]
17. Hsieh, C.C.; Lin, D.Y.; Chen, M.C.; Wu, W. Microstructure, recrystallization, and mechanical property evolutions in the heat-affected and fusion zones of the dissimilar stainless steels. *Mater. Trans.* **2007**, *48*, 2898–2902. [[CrossRef](#)]
18. Hoang, A.T.; Le, V.V.; Nguyen, A.X.; Nguyen, D.N. A study on the changes in microstructure and mechanical properties of multi-pass welding between 316 stainless steel and low-carbon steel. *J. Adv. Manuf. Technol.* **2018**, *12*, 25–40.
19. Bahador, A.; Hamzah, E.; Mamat, M.F. Effect of filler metals on the mechanical properties of dissimilar welding of stainless steel 316L and carbon steel A516 GR 70. *J. Teknol.* **2015**, *75*, 61–65. [[CrossRef](#)]
20. Vargas, V.H.; Albiter, A.; Domínguez-Aguilar, M.A.; Altamirano, G.; Maldonado, C. Corrosion resistance of dissimilar GTA welds of pipeline steel and super duplex stainless steels in synthetic brine. *Corros. Journal.* **2021**, *77*, 668–680. [[CrossRef](#)] [[PubMed](#)]
21. Wang, J.; Lu, M.-x.; Zhang, L.; Chang, W.; Xu, L.-n.; Hu, L.-h. Effect of welding process on the microstructure and properties of dissimilar weld joints between low alloy steel and duplex stainless steel. *Int. J. Miner. Metall. Mater.* **2012**, *19*, 518–524. [[CrossRef](#)]
22. Ming, H.; Zhang, Z.; Wang, J.; Han, E.-H.; Wang, P.; Sun, Z. Microstructure of a safe-end dissimilar metal weld joint (SA508-52-316L) prepared by narrow-gap GTAW. *Mater. Charact.* **2017**, *123*, 233–243. [[CrossRef](#)]
23. Zhang, R.; Wu, Q.; Wang, L.; Zeng, C.; Wang, X. Study on A-TIG welding of Q245R/321 dissimilar steel. *IOP Conf. Ser. Earth Environ. Sci.* **2019**, *310*, 042011. [[CrossRef](#)]
24. Yilmaz, R.; Tümer, M. Microstructural studies and impact toughness of dissimilar weldments between AISI 316 L and AH36 steels by FCAW. *Int. J. Adv. Manuf. Technol.* **2013**, *67*, 1433–1447. [[CrossRef](#)]
25. Afriansyah, A.A. Dissimilar metal welding using Shielded metal arc welding: A Review. *Technol. Rep. Kansai Univ.* **2020**, *64*, 1935–1948.
26. Bahandari, D.; Chhibber, R.; Arorac, N.; Mehtad, R. Investigation of TiO₂-SiO₂-CaO-CaF₂ based electrode coatings on weld metal chemistry and mechanical behaviour of bimetallic welds. *J. Manuf. Process.* **2016**, *23*, 61–74. [[CrossRef](#)]
27. Pratiwi, D.K.; Arifin, A.; Gunawan; Mardhi, A.; Afriansyah. Investigation of welding parameters of dissimilar weld of SS316 and ASTM A36 joint using a grey-based Taguchi Optimization Approach. *J. Manuf. Mater. Process.* **2023**, *7*, 39. [[CrossRef](#)]
28. Mas, F.; Tassin, C.; Roch, F.; Yescas, M.; Todeschini, P.; Bréchet, Y. Growth morphologies and primary solidification modes in a dissimilar weld between a low-alloy steel and an austenitic stainless steel. *Metals* **2018**, *8*, 284. [[CrossRef](#)]
29. Nivas, R.; Singh, P.K.; Das, G.; Das, S.K.; Kumar, S.; Mahato, B.; Sivaprasad, K.; Ghosh, M. A comparative study on microstructure and mechanical properties near interface for dissimilar materials during conventional V-groove and narrow gap welding. *J. Manuf. Process.* **2017**, *25*, 274–283. [[CrossRef](#)]
30. Asadollahi, A.; Bahrami, A.; Shamanian, M. The effects of filler metal and butter layer on the microstructure and mechanical properties of API 5L X65/AISI 304L joint. *J. Mater. Res. Technol.* **2023**, *23*, 4148–4166. [[CrossRef](#)]
31. Ghosh, P.S.; Sen, A.; Chattopadhyaya, S.; Sharma, S.; Singh, J.; Li, C.; Królczyk, G.; Rajkumar, S. Progressive developments and challenges in dissimilar laser welding of steel to various other light alloys (Al/Ti/Mg): A comprehensive review. *Heliyon* **2022**, *8*, e11710. [[CrossRef](#)]
32. Anawa, E.M.; Olabi, A.G. Optimization of tensile strength of ferritic/austenitic laser-welded components. *Opt. Lasers Eng.* **2008**, *46*, 571–577. [[CrossRef](#)]
33. Casalino, G.; Guglielmi, P.; Lorusso, V.D.; Mortello, M.; Peyrec, P.; Sorgente, D. Laser offset welding of AZ31B magnesium alloy to 316 stainless steel. *J. Mater. Process. Technol.* **2017**, *242*, 49–59. [[CrossRef](#)]
34. Pereira, A.B.; Cabrinha, A.; Rocha, F.; Marques, P.; Fernandes, F.A.O.; Alves de Sousa, R.J. Dissimilar metals laser welding between DP1000 steel and aluminum alloy 1050. *Metals* **2019**, *9*, 102. [[CrossRef](#)]
35. Zhang, M.; Chen, G.; Zhou, Y.; Liao, S. Optimization of deep penetration laser welding of thick stainless steel with a 10 kW fiber laser. *Mater. Des.* **2014**, *53*, 568–576. [[CrossRef](#)]
36. Stanciu, E.M.; Pascu, A.; Tiorean, M.H.; Roata, I.C.; Voiculescu, I.; Hulka, I.; Croitoru, C. Dissimilar laser welding of AISI 321 and AISI 1010. *Tech. Gaz.* **2018**, *25*, 344–349. [[CrossRef](#)]
37. Scutelnicu, E.; Iordachescu, M.; Rusu, C.C.; Mihailescu, D.; Ocaña, J.L. Metallurgical and mechanical characterization of low carbon steel—Stainless steel dissimilar joints made by laser autogenous welding. *Metals* **2021**, *11*, 810. [[CrossRef](#)]

38. Venkatakrisna, A.; Lakshminarayanan, A.; Vasantharaja, P.; Vasudevan, M. Decisive impact of filler-free joining processes on the Microstructural evolution, tensile and impact properties of 9Cr-1Mo-V-Nb to 316 L(N) dissimilar joints. *Proc. Inst. Mech. Eng. Part C J. Mech. Eng. Sci.* **2022**, *236*, 2408–2427. [[CrossRef](#)]
39. Danielewski, H.; Skrzypczyk, A.; Tofil, S.; Witkowski, G.; Rutkowski, S. Numerical Simulation of Laser Welding Dissimilar Low Carbon and Austenitic Steel Joint. *Open Eng.* **2020**, *10*, 491–498. [[CrossRef](#)]
40. Hamada, A.; Ghosh, S.; Ali, M.; Jaskari, M.; Järvenpää, A. Studying the strengthening mechanisms and mechanical properties of dissimilar laser-welded butt joints of medium-Mn stainless steel and automotive high-strength carbon steel. *Mater. Sci. Eng. A* **2022**, *856*, 143936. [[CrossRef](#)]
41. Hamada, A.; Khosravifard, A.; Ali, M.; Ghosh, S.; Jaskari, M.; Hietala, M.; Järvenpää, A.; Newishy, M. Micromechanical analysis and finite element modelling of laser-welded 5-mm-thick dissimilar joints between 316L stainless steel and low-alloyed ultra-high-strength steel. *Mater. Sci. Eng. A* **2023**, *882*, 145442. [[CrossRef](#)]
42. Prabakaran, M.P.; Kannan, G.R. Optimization of laser welding process parameters in dissimilar joint of stainless steel AISI316/AISI1018 low carbon steel to attain the maximum level of mechanical properties through PWHT. *Opt. Laser Technol.* **2019**, *112*, 314–322. [[CrossRef](#)]
43. Prabakaran, M.P.; Kannan, G.R. Effects of post-weld heat treatment on dissimilar laser welded joints of austenitic stainless steel to low carbon steel. *Int. J. Press. Vessel. Pip.* **2021**, *191*, 104322. [[CrossRef](#)]
44. Liu, F.; Zhou, X.; Chen, X.; Gong, X.; Wu, L.; Chen, B.; Chen, K.; Tan, C. Melt flowing behaviors and microstructure evolution during laser offset welding of dissimilar metals between AH36 and 304 steels. *Opt. Laser Technol.* **2022**, *151*, 10802. [[CrossRef](#)]
45. Li, G.; Zhang, C.; Gao, M.; Zeng, X. Role of arc mode in laser-metal active gas arc hybrid welding of mild steel. *Mater. Des.* **2014**, *61*, 239–250. [[CrossRef](#)]
46. Russo Spina, P.; Angelastro, A.; Casalino, G. Hybrid laser arc welding of dissimilar TWIP and DP high strength steel weld. *J. Manuf. Process.* **2019**, *39*, 233–240. [[CrossRef](#)]
47. Zhang, X.; Mi, G.; Wang, C. Microstructure and performance of hybrid laser-arc welded high-strength low alloy steel and austenitic stainless steel dissimilar joint. *Opt. Laser Technol.* **2020**, *122*, 105878. [[CrossRef](#)]
48. Missori, S.; Sili, A. Prediction of weld metal microstructure in laser beam welded clad steel. *Metallurgist* **2018**, *62*, 84–92. [[CrossRef](#)]
49. Salminen, A. The filler wire—Laser beam interaction during laser welding with low alloyed steel filler wire. *Mechanika* **2010**, *84*, 67–74.
50. Yu, W.X.; Liu, B.X.; Chen, C.X.; Liu, M.Y.; Zhang, X.; Fang, W.; Ji, P.G.; He, J.N.; Yin, F.X. Microstructure and mechanical properties of stainless steel clad plate welding joints by different welding processes. *Sci. Technol. Weld. Join.* **2020**, *25*, 571–580. [[CrossRef](#)]
51. Hansen, K.S.; Olsen, F.O.; Kristiansen, M.; Madsen, O. Joining of multiple sheets in a butt-joint configuration using single pass laser welding with multiple spots. *J. Laser Appl.* **2015**, *27*, 032011. [[CrossRef](#)]
52. Kristiansen, M.; Hansen, K.S.; Langbak, A.; Johansen, S.B.; Krempin, S.B.; Hornum, M.D. Single pass laser welding with multiple spots to join four sheets in a butt-joint configuration. *Phys. Procedia* **2017**, *89*, 205–213. [[CrossRef](#)]
53. Cui, L.; Chen, H.; Chen, B.; He, D. Welding of dissimilar steel/Al Joints using dual-beam lasers with side-by-side configuration. *Metals* **2018**, *8*, 1017. [[CrossRef](#)]
54. Xu, S. Thermal stress analysis of dissimilar welding joints by finite element method. *Procedia Eng.* **2011**, *15*, 3860–3864. [[CrossRef](#)]
55. Bharthi, A.D.; Babu, U.H. Structural and Thermal Analysis of Dissimilar Metal Welding of 1020 Mild Steel and 304 Stainless Steel. *Int. J. Sci. Eng. Technol. Res.* **2015**, *4*, 1761–1771.
56. An, G.; Park, J.; Lim, W.; Park, H.; Han, I. Characteristics of welding residual stress distribution in dissimilar weld joints. *Metals* **2022**, *12*, 405. [[CrossRef](#)]
57. Dokme, F.; Kulekci, M.K.; Esme, U. Microstructural and mechanical characterization of dissimilar metal welding of Inconel 625 and AISI 316L. *Metals* **2018**, *8*, 797. [[CrossRef](#)]
58. Ramkumar, T.; Selvakumar, M.; Narayanasamy, P.; Ayisha Begam, A.; Mathavand, P.; Arun Raj, A. Studies on the structural property, mechanical relationships and corrosion behaviour of Inconel 718 and SS 316L dissimilar joints by TIG welding without using activated flux. *J. Manuf. Proc.* **2017**, *30*, 290–298. [[CrossRef](#)]
59. Shankar, V.; Gill, T.P.S.; Mannan, S.L.; Sundaresan, S. Solidification Cracking in Austenitic Stainless Steel Welds. *Sadhana Acad. Proc. Eng. Sci.* **2003**, *28*, 359–382.
60. Manitsas, D.; Andersson, J. Hot Cracking Mechanisms in Welding Metallurgy: A Review of Theoretical Approaches. In Proceedings of the ICEAF-V, Chios Island, Greece, 22–28 June 2018.
61. Fei, Z.; Pan, Z.; Cui, D.; Li, H.; Van Duin, S.; Yu, Z. Microstructural characterization and mechanical properties of K-TIG welded SAF2205/AISI316L dissimilar joint. *J. Manuf. Process.* **2019**, *45*, 340–355. [[CrossRef](#)]
62. Landowski, M.; Swierczynska, A.; Rogalski, G.; Fydrych, D. Autogenous fiber laser welding of 316L austenitic and 2304 lean duplex stainless steels. *Materials* **2020**, *13*, 2930. [[CrossRef](#)]
63. Alali, M.; Abass, M.H.; Abbas, W.S.; Shehab, A.A. Effect of nickel powder buffering layer on microstructure and hardness properties of high carbon steel/stainless steel arc stud welding. *Mater. Res.* **2020**, *23*, e20190567. [[CrossRef](#)]
64. Giudice, F.; Sili, A. Weld metal microstructure prediction in laser beam welding of austenitic stainless steel. *Appl. Sci.* **2021**, *11*, 1463. [[CrossRef](#)]
65. Tandon, V.; Patil, A.P.; Kowshik, S. Impact of filler electrodes on welding properties of dissimilar welded 316L/201 austenitic stainless steels. *Eng. Proc.* **2023**, *59*, 90. [[CrossRef](#)]

66. Wu, C.; Li, S.; Zhang, C.; Wang, X. Microstructural evolution in 316LN austenitic stainless steel during solidification process under different cooling rates. *J. Mater. Sci.* **2016**, *51*, 2529–2539. [[CrossRef](#)]
67. Zhai, R.; Zhang, H.; Xu, B.; Liu, S.; Xie, B.; Sun, M. Elimination of δ -ferrite in N50 steel and its effect on cryogenic mechanical properties. *Cryogenics* **2022**, *126*, 103522. [[CrossRef](#)]
68. Bunaziv, I.; Olden, V.; Akselsen, O.M. Metallurgical Aspects in the Welding of Clad Pipelines—A Global Outlook. *Appl. Sci.* **2019**, *9*, 3118. [[CrossRef](#)]
69. Valiente Bermejo, M.A. Reagent selection in austenitic stainless steel solidification modes characterization. *Weld. J.* **2012**, *91*, 133s–139s.
70. Yu, P.; Thompson, K.J.; MCCarthy, J.; Kou, S. Microstructure evolution and solidification cracking in austenitic stainless steel. *Welds. Weld. J.* **2018**, *97*, 301s–314s. [[CrossRef](#)]
71. Tandon, V.; Thombre, M.A.; Patil, A.P.; Taiwade, R.V.; Vashishtha, H. Effect of Heat Input on the Microstructural, mechanical, and corrosion properties of dissimilar weldment of conventional austenitic stainless steel and low-nickel stainless steel. *Metallogr. Microstruct. Anal.* **2020**, *9*, 668–677. [[CrossRef](#)]
72. Li, Y.; Luo, Y.; Li, J.; Song, D.; Xu, B.; Chen, X. Ferrite formation and its effect on deformation mechanism of wire arc additive manufactured 308 L stainless steel. *J. Nucl. Mater.* **2021**, *550*, 152933. [[CrossRef](#)]
73. Zhou, C.; Dia, P.; Wu, H.; He, M.; Liu, X.; Chu, P.K. Effect of the ferrite morphology on hydrogen embrittlement of MAG welded 304 austenitic stainless steel. *Appl. Surf. Sci.* **2022**, *606*, 154866. [[CrossRef](#)]
74. Wang, Q.; Chen, S.; Rong, L. Properties of heavy-section AISI 316 stainless steel casting. *Met. Mater. Trans.* **2020**, *51*, 2998–3008. [[CrossRef](#)]
75. Weman, K. *Welding Processes Handbook*; Woodhead Publishing Ltd.: Abington, PA, USA; Cambridge, UK, 2003; pp. 149–150.
76. Chuaiphon, W.; Kumkoon, P.; Kalnaowakul, P. Dissimilar welding of AISI 201 and 202 low nickel stainless steels by GTA and PA welding processes. *J. Alloys Metall. Syst.* **2023**, *4*, 100047. [[CrossRef](#)]
77. Unnikrishnan, R.; Satish Indury, K.S.N.; Ismail, T.P.; Bhadauria, A.; Shekhawat, S.K.; Khatirkar, R.K.; Sanjay, G.S. Effect of heat input on the microstructure, residual stresses and corrosion resistance of 304L austenitic stainless steel weldments. *Mater. Charact.* **2014**, *93*, 10–23. [[CrossRef](#)]
78. Vitek, J.M.; David, S.A.; Hinman, C.R. Improved Ferrite Number Prediction Model That Accounts for Cooling Rate Effects—Part 2: Model Results. *Weld. J.* **2003**, *82*, 43s–50s.
79. DuPont, J.N. Fundamentals of weld solidification. In *Metals Handbook*, 1st ed.; Lienert, T.J., Babu, S.S., Siewert, T.A., Acoff, V.L., Eds.; ASM: Materials Park, OH, USA, 2011; Volume 06A, pp. 96–114.
80. Ghosh, A.; Misra, D.; Acharyya, S.K. Experimental and numerical investigation on laser welding of 2205 duplex stainless steel. *Lasers Manuf. Mater. Process.* **2019**, *6*, 228–246. [[CrossRef](#)]
81. Kik, T. Heat source models in numerical simulations of laser welding. *Materials* **2020**, *13*, 2653. [[CrossRef](#)] [[PubMed](#)]
82. Giudice, F.; Missori, S.; Sili, A. Parameterized multipoint-line analytical modeling of a mobile heat source for thermal field prediction in laser beam welding. *Int. J. Adv. Manuf. Technol.* **2021**, *112*, 1339–1358. [[CrossRef](#)]
83. Giudice, F.; Sili, A. Validation of a theoretical model for laser welding thermal field by multi-physics numerical simulation. *Metals* **2023**, *13*, 2020. [[CrossRef](#)]
84. Gajjar, P.K.; Khatri, B.C.; Siddhpura, A.; Siddhpura, M.A. Sensitization and desensitization (healing) in austenitic stainless steel: A Critical Review. *Trans. Indian Inst. Met.* **2022**, *75*, 1411–1427. [[CrossRef](#)]
85. Ramdan, R.D.; Kariem, M.A.; Neswan, O.; Wirawan, F.; Suratman, R.; Widyanto, B.; Wirawan, R. Mechanical properties and microstructure at stainless steel HAZ from dissimilar metal welding after heat treatment processes. *IOP Conf. Ser. Mater. Sci. Eng.* **2019**, *553*, 012034. [[CrossRef](#)]
86. Dai, P.; Li, S.; Wu, L.; Wang, Y.; Feng, G. Dean Deng A new numerical model to predict welding-induced sensitization in SUS304 austenitic stainless steel joint. *J. Mater. Res. Technol.* **2022**, *17*, 234–243. [[CrossRef](#)]
87. Winarto, W.; Anis, M.; Riastuti, R.; Suarjana, I.N. Study the effect of welding position and plate thickness to the mechanical and microstructural properties of the TIG dissimilar metal welded between carbon steel ASTM A36 and stainless steel 304 plates. *Mater. Sci. Forum* **2020**, *1000*, 364–372. [[CrossRef](#)]
88. DuPont, J.N. Microstructural evolution and high temperature failure of ferritic to austenitic dissimilar welds. *Int. Mater. Rev.* **2012**, *57*, 208–231. [[CrossRef](#)]
89. Nimko, M.O. Influence of welding parameters on decarburization in heat affected zone of dissimilar weldments after post weld heat treatment. *Arch. Mater. Sci. Eng.* **2021**, *112*, 23–31. [[CrossRef](#)]
90. Britto, J.G.; Sulbihar, A.D.; Dinesh, K.L.; Jeya, J.; Durai, R.R.B.; Sriram, V. Microstructural studies of P91 and SS304L dissimilar welding. *Mater. Today Proc.* **2021**, *47*, 4571–4577. [[CrossRef](#)]

Disclaimer/Publisher's Note: The statements, opinions and data contained in all publications are solely those of the individual author(s) and contributor(s) and not of MDPI and/or the editor(s). MDPI and/or the editor(s) disclaim responsibility for any injury to people or property resulting from any ideas, methods, instructions or products referred to in the content.